Supporting information

Experimental Considerations. All manipulations were performed under an argon atmosphere (or nitrogen atmosphere where specified) by Schlenk techniques or in an M. Braun glovebox maintained at or below 1 ppm of O_2 and H_2O. Glassware was dried at 150 °C overnight, and Celite was dried overnight at 200 °C under vacuum. Pentane, hexane, benzene, diethyl ether, and toluene were purified by passage through activated alumina and Q5 columns from Glass Contour Co, under Ar. THF was distilled under Ar from a potassium benzophenone ketyl solution. All solvents were stored over 3 Å molecular sieves. Benzene-d_6 was dried and stored over flame-activated alumina. THF-d_8 was vacuum transferred from sodium benzophenone ketyl solutions and was stored over 3 Å molecular sieves. Before use, an aliquot of each solvent was tested with a drop of sodium benzophenone ketyl in THF solution. Pyridine and pyridine-d_5 were dried and stored over 3 Å molecular sieves. The starting material $LFe(C_6H_6)$ was synthesized according to the literature procedure (K. C. MacLeod, D. J. Vinyard and P. L. Holland, *J. Am. Chem. Soc.*, 2014, in press.)

NMR data were collected on an Agilent DD2 400 MHz spectrometer. Chemical shifts in ^{1}H NMR spectra are referenced to external $SiMe_4$ using the residual protio solvent peaks as internal standards: THF-d_8 (3.57 ppm), pyridine-d_5 (7.22 ppm), C_6D_6 (7.16 ppm), and C_6D_{12} (1.38 ppm). Elemental analyses were performed at the CENTC Elemental Analysis Facility at the University of Rochester. IR spectroscopy was run on an Alpha Platinum ATR IR Spectrometer. Mössbauer data were recorded on a spectrometer with alternating constant acceleration. Mössbauer measurements were performed using a SEE Co. MS4 Mössbauer spectrometer integrated with a Janis SVT-400T He/N_2 cryostat for measurements at 80 K with a 0.07 T applied magnetic field. Isomer shifts were determined relative to α-Fe at 298 K. All Mössbauer spectra were fit using the program WMoss (SEE Co.).

$LFe(Py)(\mu\text{-}C_{10}H_{10}N_2)(Py)FeL$ ($\mathbf{1_2}$). $LFe(C_6H_6)$ (252.5 mg, 0.5574 mmol) was dissolved in Et_2O (2 mL). To this stirring solution was added pyridine (112 μL, 1.40 mmol). Immediately upon addition of pyridine, the solution turned a green color. The solution was stirred at 25 °C for 16 h. Bright red solid was observed in the reaction vial. Pentane (2 mL) was layered upon the solution and stored at -40 °C for 24 h. This gave a bright red solid of $\mathbf{1_2}$ (214.5 mg, 71.8%). Anal. Calcd for $Fe_2N_8C_{64}H_{74}$: C, 72.04; H, 6.99; N, 10.50. Found: C, 72.01; H, 7.58; N, 9.90. ^{1}H NMR (pyridine-d_5, 25 °C, 400 MHz): δ 123 (s, 3H, γ-CH_3, $\mathbf{1_1}$), 25.7 (s, 4H, meta-CH, $\mathbf{1_1}$), 22.2 (s, 12H, ortho-CH_3, $\mathbf{1_1}$), -41.5 (s, 2H, para-CH, $\mathbf{1_1}$), -117 (s, 6H, β-CH_3, $\mathbf{1_1}$); 154 (br s, 3H, γ-CH_3, $\mathbf{1_2}$), 27.6 (s, 4H, meta-CH, $\mathbf{1_2}$), 23.6 (s, 12H, ortho-CH_3, $\mathbf{1_2}$), -57.5 (s, 2H, para-CH, $\mathbf{1_2}$), -97.9 (s, 6H, β-CH_3, $\mathbf{1_2}$) ppm. IR (neat, cm^{-1}): 3061(w), 3018(w), 2959(w), 2916(w), 2848(w), 2808(w), 2759(w), 1631(m), 1599(w), 1562(w), 1521(m), 1480(sh w), 1462(m), 1444(m), 1438(sh m), 1407(m), 1364(m), 1340(s), 1291(sh m), 1279(m), 1254(w), 1228(w), 1207(w), 1191(s), 1152(w), 1120(w), 1095(w), 1069(w), 1036(sh w), 1028(m), 981(s), 950(sh w), 932(w),

916(w), 885(w), 858(w), 797(w), 756(m), 734(m), 701(m), 681(w), 634(m), 628(m), 587(w), 506(sh w), 493(w), 420(w). Evans' Method (pyridine-d_5, moment per iron, MW: 453.4): (-33.2 °C) 5.4±0.1, (22.1 °C) 5.4±0.1, (**1**$_1$, 78.3°C) 5.1±0.2 μ_B.

LFe(Py)(μ-Py)FeL (2). LFe(C_6H_6) (234.0 mg, 0.5166 mmol) was dissolved in Et_2O (2 mL). To this stirring solution was added pyridine (46.0 μL, 0.570 mmol). The solution immediately turned a red-brown color. The solution was stirred for 4 hours, and then pentane (10 mL) was added and the solution was filtered through a plug of Celite (0.5 cm x 2 cm). This solution was cooled to -40 °C for 24 h to precipitate a purple solid (72.2 mg, 30.5%). Anal. Calcd for $Fe_2N_6C_{54}H_{64}\cdot C_5H_{12}$: C, 72.24; H, 7.81; N, 8.57. Found: C, 71.87; H, 7.50; N, 8.74. ^{1}H NMR (THF-d_8, 25 °C, 400 MHz): δ 172 (s, 3H, γ-CH_3), 77.9 (s, 3H, γ-CH_3), 37.6 (br s, 6H, ortho-CH_3 or β-CH_3), 27.7 (s, 4H, meta-CH), 17.3 (s, 4H, meta-CH), 13.1 (s, 12H, 2 x ortho-CH_3 or β-CH_3), -9.8 (s, 2H, para-CH), -59.7 (s, 2H, para-CH), -63.2 (s, 6H, β-CH_3), -102.6 (s, 6H, β-CH_3) ppm. IR (neat, cm^{-1}): 3064(w), 3013(w), 2953(w), 2914(w), 2853(w), 1642(w), 1591(w), 1576(w), 1521(m), 1482(sh w), 1464(m), 1442(m), 1405(m), 1395(sh m), 1364(m), 1340(vs), 1285(m), 1258(w), 1213(w), 1191(s), 1160(w), 1130(w), 1097(m), 1089(m), 1066(w), 1028(w), 987(m), 956(m), 944(m), 918(w), 891(w), 859(w), 799(w), 771(sh m), 761(s), 716(m), 704(m), 634(w), 608(w), 600(w), 571(w), 518(w), 493(w), 456(w), 422(w). Evans' Method (THF-d_8 + 0.0536 M pyridine, moment per iron, MW: 453.4): 4.5 ± 0.1 B.M.

Dissolution of LFe(μ-C_6H_6) in neat pyridine-d_5:

LFe(C_6H_6) (7.2 mg, 0.016 mmol) was dissolved in ~700 μL of pyridine-d_5 to give a red solution. ^{1}H NMR (pyridine-d_5, 25 °C, 400 MHz): δ 154 (br s, 3H, γ-CH_3, **1**$_2$), 123 (s, 3H, γ-CH_3, **1**$_1$), 27.6 (s, 4H, meta-CH, **1**$_2$), 25.7 (s, 4H, meta-CH, **1**$_1$), 23.6 (s, 12H, ortho-CH_3, **1**$_2$), 22.2 (s, 12H, ortho-CH_3, **1**$_1$), -41.5 (s, 2H, para-CH, **1**$_1$), -57.5 (s, 2H, para-CH, **1**$_2$), -97.9 (s, 6H, β-CH_3, **1**$_2$), -117 (s, 6H, β-CH_3, **1**$_1$).

Crystallographic details

Low-temperature diffraction data (ω-scans) were collected on a Rigaku MicroMax-007HF diffractometer coupled to a Saturn994+ CCD detector with Cu Kα (λ = 1.54178 Å) for the structures of **1**$_2$ and **2.** All structures were solved by direct methods using SHELXS and were refined against F^2 on all data by full-matrix least squares with SHELXL (Sheldrick, G. M. *Acta Cryst.* **2008**, *A64*, 112–122). All non-hydrogen atoms were refined anisotropically. Unless otherwise noted, hydrogen atoms were included in the model at geometrically calculated positions and refined using a riding model. The isotropic displacement parameters of all hydrogen atoms were fixed to 1.2 times the *U* value of the atoms to which they are linked (1.5 times for methyl groups). All disorder was refined with similarity restraints on the 1,2- and 1,3-distances and displacement parameters. CCDC numbers 1012694 and 1012702 contain the supplementary crystallographic data for this paper. These data can be obtained free of charge from The Cambridge Crystallographic Data Center via www.ccdc.cam.ac.uk/data_request/cif.

Crystal Data for $\mathbf{1_2}$

There appear to be two species of pyridine molecules coordinated to Fe1 and Fe2: two discrete, uncoupled pyridine molecules, and the coupled species joined at the *para* positions. The uncoupled and coupled species are in relative occupancies of 0.42 and 0.58, respectively. The atoms in the minor and major forms are {C2B, C3B, C4B, C5B, C7B, C8B, C9B} and {C24, C34, C44, C54, C74, C84, C94}, where atoms {C64, C10B} are shared between both models.

Table S1. Crystal data and structure refinement for $\mathbf{1_2}$.

Empirical formula	$C_{145}H_{183}Fe_4N_{17}O_3$	
Formula weight	2435.47	
Temperature	93(2) K	
Wavelength	1.54187 Å	
Crystal system	Orthorhombic	
Space group	*P c a* 2_1	
Unit cell dimensions	a = 27.6897(2) Å	α = 90°
	b = 11.5655(5) Å	β = 90°
	c = 42.052(3) Å	γ = 90°
Volume	13467.1(11) $Å^3$	
Z	4	
Density (calculated)	1.201 Mg/m^3	
Absorption coefficient	3.832 mm^{-1}	
F(000)	5200	
Crystal color	Red	
Crystal size	0.050 x 0.030 x 0.030 mm^3	
Θ range for data collection	2.101 to 65.086°	
Index ranges	$-32 \le h \le 32$, $-13 \le k \le 13$, $-49 \le l \le 49$	
Reflections collected	447121	
Independent reflections	22989 [R(int) = 0.2488]	
Completeness to θ = 67.687°	94.5 %	
Absorption correction	Semi-empirical from equivalents	
Max. and min. transmission	0.894 and 0.630	
Refinement method	Full-matrix least-squares on F^2	
Data / restraints / parameters	22989 / 765 / 1621	
Goodness-of-fit on F^2	0.947	
Final R indices [I>2σ(I) = 12937 data]	R1 = 0.0756, wR2 = 0.1701	
R indices (all data)	R1 = 0.1250, wR2 = 0.2021	
Absolute structure parameter	0.083(3)	
Extinction coefficient	0.00137(9)	
Largest diff. peak and hole	0.556 and -0.397 e.$Å^{-3}$	

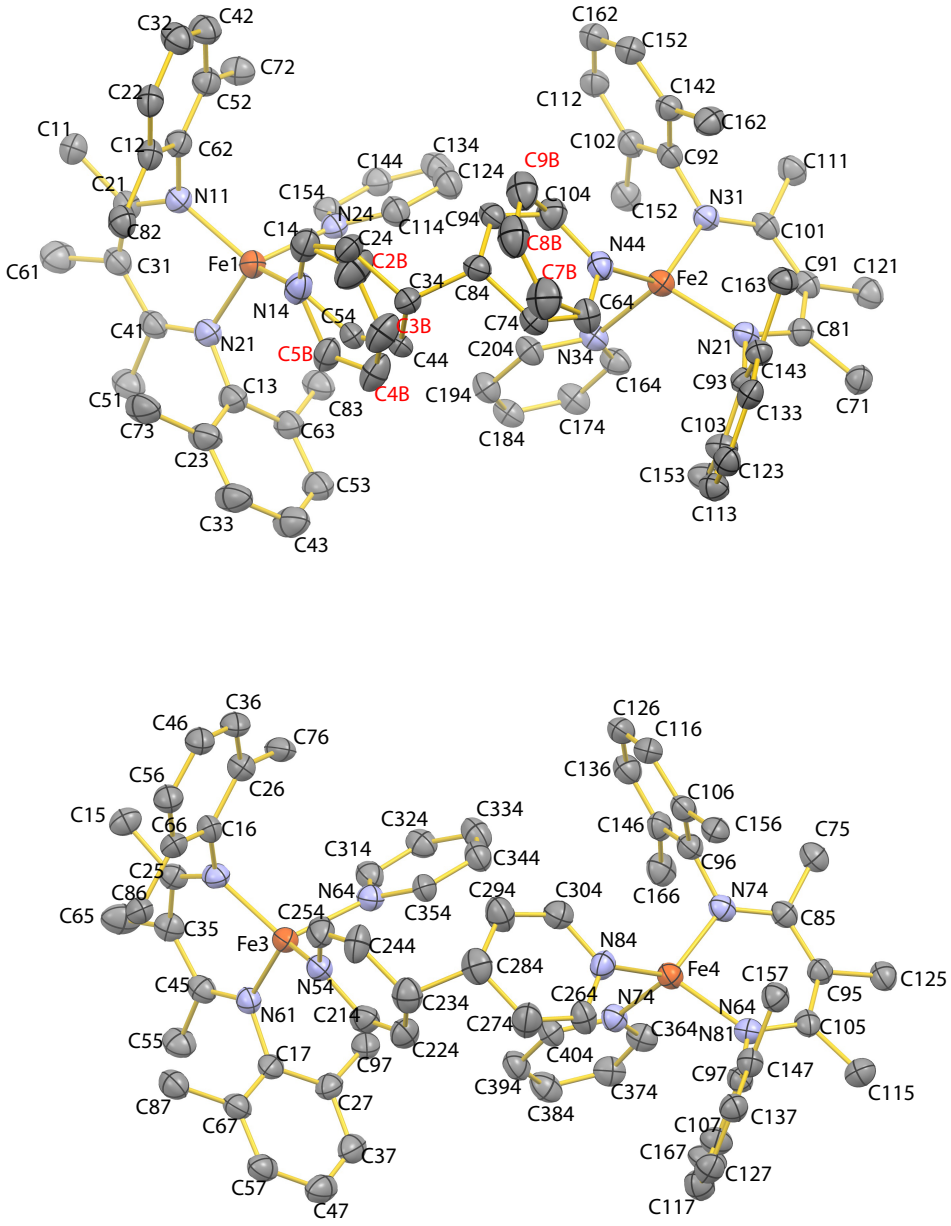

Figure S1. The full numbering scheme of the two crystallographically independent iron complexes contained in complex $\mathbf{1}_2$. The unbridged pyridines are highlighted with red labels. Atoms {C24, C34, C44, C54, C74, C84, C94} and {C2B, C3B, C4B, C5B, C7B, C8B, C9B} have site occupacy factors of 0.58 and 0.42, respectively. All atoms shown are depicted with 25% thermal contours. The hydrogen atoms and solvent molecules are omitted for clarity.

Crystal Data for Complex **2**

Atoms H25, H35, and H45 refined semi-freely. A disordered *n*-pentane was located at the crystallographic inversion center. The thermal parameters of the disordered solvent molecule were restrained to be similar to each other.

Table S2. Crystal data and structure refinement for **2**.

Empirical formula	$C_{56.50}H_{70}Fe_2N_6$	
Formula weight	944.88	
Temperature	93(2) K	
Wavelength	1.54187 Å	
Crystal system	Monoclinic	
Space group	$P2_1/n$	
Unit cell dimensions	a = 15.9655(3) Å	α = 90°
	b = 14.7809(3) Å	β = 104.422(7)°
	c = 21.7126(15) Å	γ = 90°
Volume	4962.4(4) $Å^3$	
Z	4	
Density (calculated)	1.265 Mg/m^3	
Absorption coefficient	5.011 mm^{-1}	
F(000)	2012	
Crystal color	Colorless	
Crystal size	0.200 x 0.190 x 0.170 mm^3	
Θ range for data collection	3.097 to 66.602°	
Index ranges	$-18 \le h \le 18$, $-17 \le k \le 16$, $-25 \le l \le 25$	
Reflections collected	115206	
Independent reflections	8733 [R(int) = 0.0592]	
Completeness to θ = 66.602°	99.9 %	
Absorption correction	Semi-empirical from equivalents	
Max. and min. transmission	0.483 and 0.398	
Refinement method	Full-matrix least-squares on F^2	
Data / restraints / parameters	8733 / 31 / 629	
Goodness-of-fit on F^2	1.108	
Final R indices [$I>2\sigma(I)$ = 7916 data]	R1 = 0.0361, wR2 = 0.0916	
R indices (all data)	R1 = 0.0402, wR2 = 0.0943	
Largest diff. peak and hole	0.372 and -0.363 $e.Å^{-3}$	

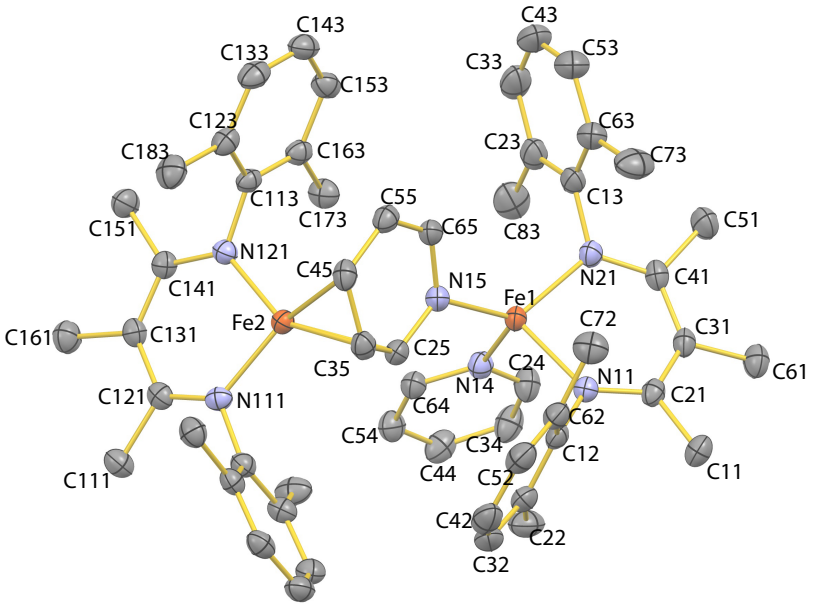

Figure S2. The full numbering scheme of **2·(C_5H_{12})**. All atoms shown are depicted with 50% thermal contours. The hydrogen atoms and solvent molecule are omitted for clarity.

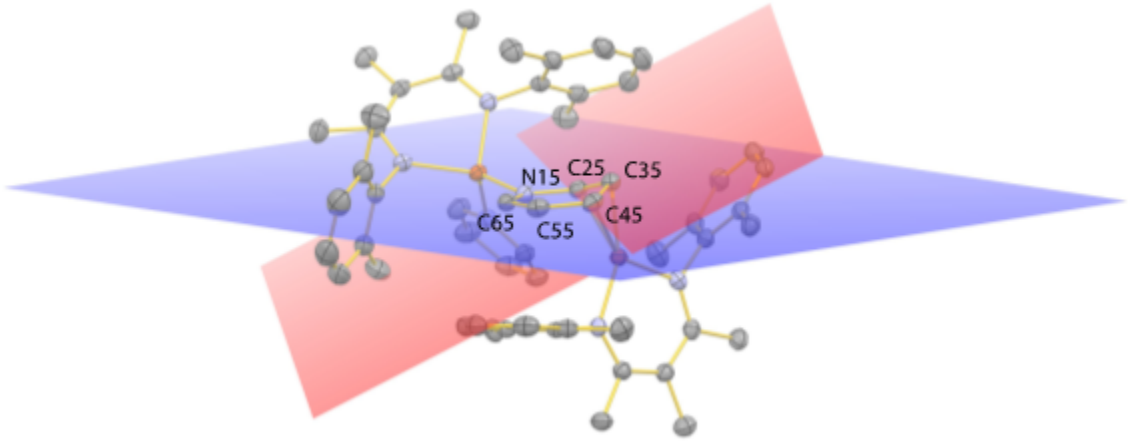

Figure S3. A thermal ellipsoid plot of **2**. The plane that contains atoms C25, C35, and C45 is shown in red; the plane that contains atoms N15, C55, and C56 is shown in blue. The acute angle between the two planes is 26.0°. All atoms are shown at 50% thermal contours, and the hydrogen atoms have been removed for clarity.

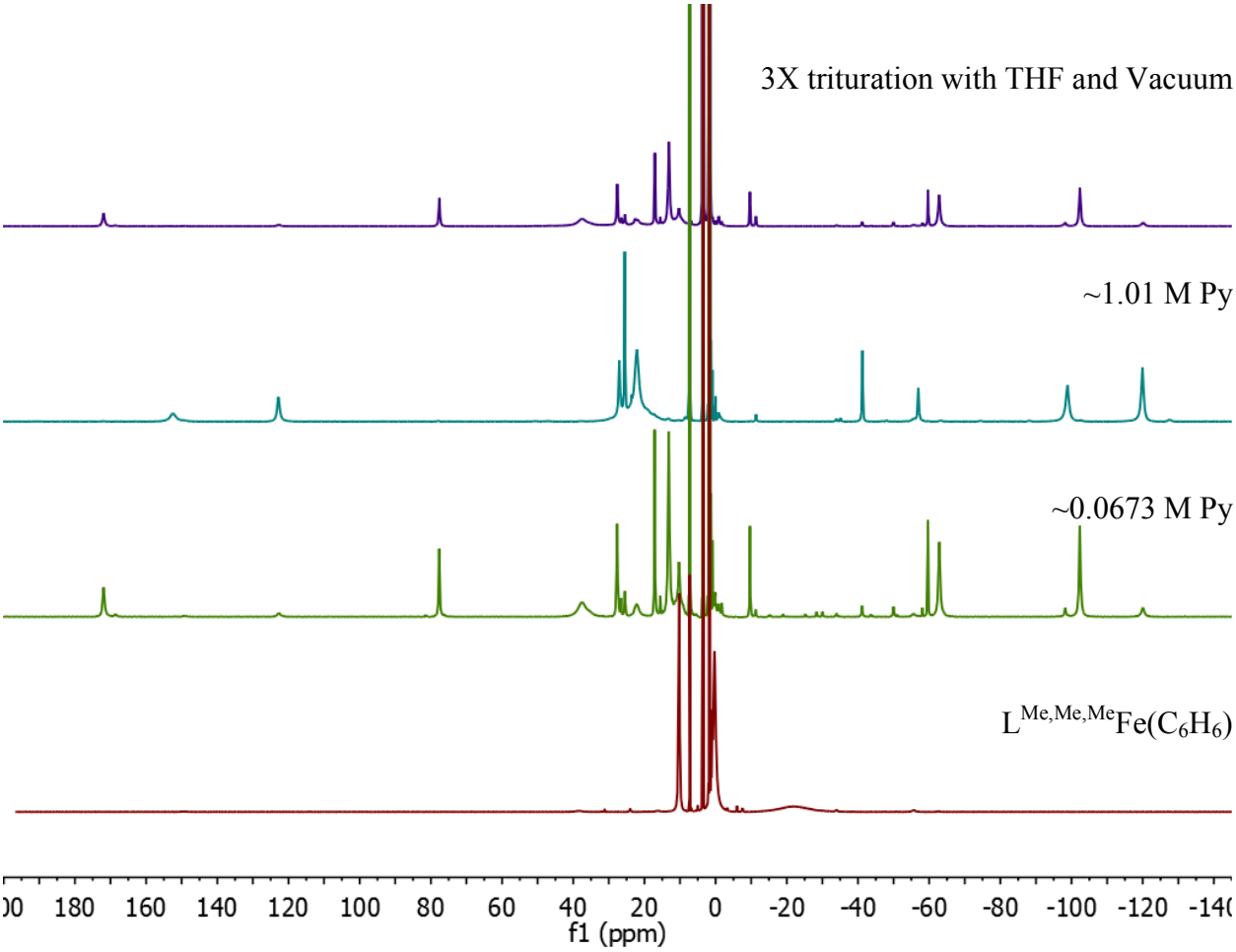

Figure S4. ^{1}H NMR spectrum of LFe(C_6H_6) with different amounts of pyridine added to the sample. After adding additional pyridine, the 0.0673 M pyridine spectrum can be reobtained by removing the solvent under vacuum and triturating it with THF three times.

Titration of pyridine-d_5 into LFe(C_6H_6) in THF-d_8:

LFe(C_6H_6) (21.2 mg, 0.047 mmol) was dissolved in ~700 µL of THF-d_8 yielding a brown solution. To this NMR solution, was added 1.8 µL pyridine (0.0235 mmol, 0.5 equiv) via syringe. The solution immediately became red/brown in color. A ^{1}H NMR spectrum was collected. ^{1}H NMR (0.5 equiv pyridine, THF-d_8, 25 °C, 400 MHz): δ 171.12, 76.79, 36.97, 27.01, 16.42, 13.14, -8.88, -22.60, -59.05, -62.77, -101.87.

Upon addition of 3.8 μL of pyridine, the solution remained red/brown in color. A ^{1}H NMR spectrum was collected. ^{1}H NMR (0.0673 M pyridine, THF-d_8, 25 °C, 400 MHz): δ171.93 (s, 3H, γ-CH_3, **2**), 122.68 (s, 3H, γ-CH_3, $\mathbf{1_2}$), 77.67 (s, 3H, γ-CH_3, **2**), 37.71 (br s, 6H, ortho-CH_3, **2**), 27.66 (s, 4H, meta-CH, **2**) , 27.58 (s, 4H, meta-CH, $\mathbf{1_2}$) , 25.50 (s, 4H, meta-CH, $\mathbf{1_1}$), 22.19 (s, 12H, ortho-CH_3, $\mathbf{1_1}$ & $\mathbf{1_2}$), 17.11 (s, 4H, meta-CH, **2**), 13.14 (s, 12H, ortho-CH_3, **2**), 10.29 (LFe(C_6H_6)), 0.31 (LFe(C_6H_6)), -9.66 (s, 2H, para-CH, **2**), -41.15 (s, 2H, para-CH. $\mathbf{1_1}$), -58.08 (s, 2H, para-CH, $\mathbf{1_2}$), -59.65 (s, 2H, para-CH, **2**), -62.85 (s, 6H, β-CH_3, **2**), -98.21 (s, 6H, β-CH_3, $\mathbf{1_2}$), -102.34 (s, 6H, β-CH_3, **2**), -120.13 (s, 6H, β-CH_3, $\mathbf{1_1}$).

Upon addition of 57 μL of pyridine, the solution remained red/brown in color. A ^{1}H NMR spectrum was collected. ^{1}H NMR (1.01 M pyridine, THF-d_8, 25 °C, 400 MHz): 152.59 (s, 3H, γ-CH_3, $\mathbf{1_2}$), 122.76 (s, 3H, γ-CH_3, $\mathbf{1_1}$), 27.03 (s, 4H, meta-CH, **2**) , 25.54 (s, 4H, meta-CH, $\mathbf{1_1}$), 22.10 (s, 12H, ortho-CH_3, **1**& $\mathbf{1_2}$), -41.24 (s, 2H, para-CH. **2**), -56.96 (s, 2H, para-CH, $\mathbf{1_2}$), -99.90 (s, 6H, β-CH_3, $\mathbf{1_2}$), -119.93 (s, 6H, β-CH_3, **1**).

The solvent was removed under vacuum and the reaction was redissolved into THF (~2 mL) three times and pumped down. It was finally redissolved into THF-d_8 (~ 700 μL). A ^{1}H NMR spectrum was collected. ^{1}H NMR (THF-d_8, 25 °C, 400 MHz): δ171.96 (s, 3H, γ-CH_3, **2**), 122.66 (s, 3H, γ-CH_3, $\mathbf{1_1}$), 77.62 (s, 3H, γ-CH_3, **2**), 37.50 (br s, 6H, ortho-CH_3 or b-CH_3, **2**), 27.62 (s, 4H, meta-CH, **2**) , 26.52 (s, 4H, meta-CH, $\mathbf{1_2}$) , 25.48 (s, 4H, meta-CH, $\mathbf{1_1}$), 22.19 (s, 12H, ortho-CH_3, $\mathbf{1_1}$ & $\mathbf{1_2}$), 17.06 (s, 4H, meta-CH, **2**), 13.11 (s, 12H, ortho-CH_3, **2**), 10.29 (LFe(C_6H_6)), -10.29 (s, 2H, para-CH, **2**), -41.20 (s, 2H, para-CH. $\mathbf{1_1}$), -58.13 (s, 2H, para-CH, $\mathbf{1_2}$), -59.69 (s, 2H, para-CH, **2**), -62.82 (s, 6H, β-CH_3, **2**), -98.31 (s, 6H, β-CH_3, $\mathbf{1_2}$), -102.36 (s, 6H, β-CH_3, **2**), -120.05 (s, 6H, β-CH_3, $\mathbf{1_1}$).

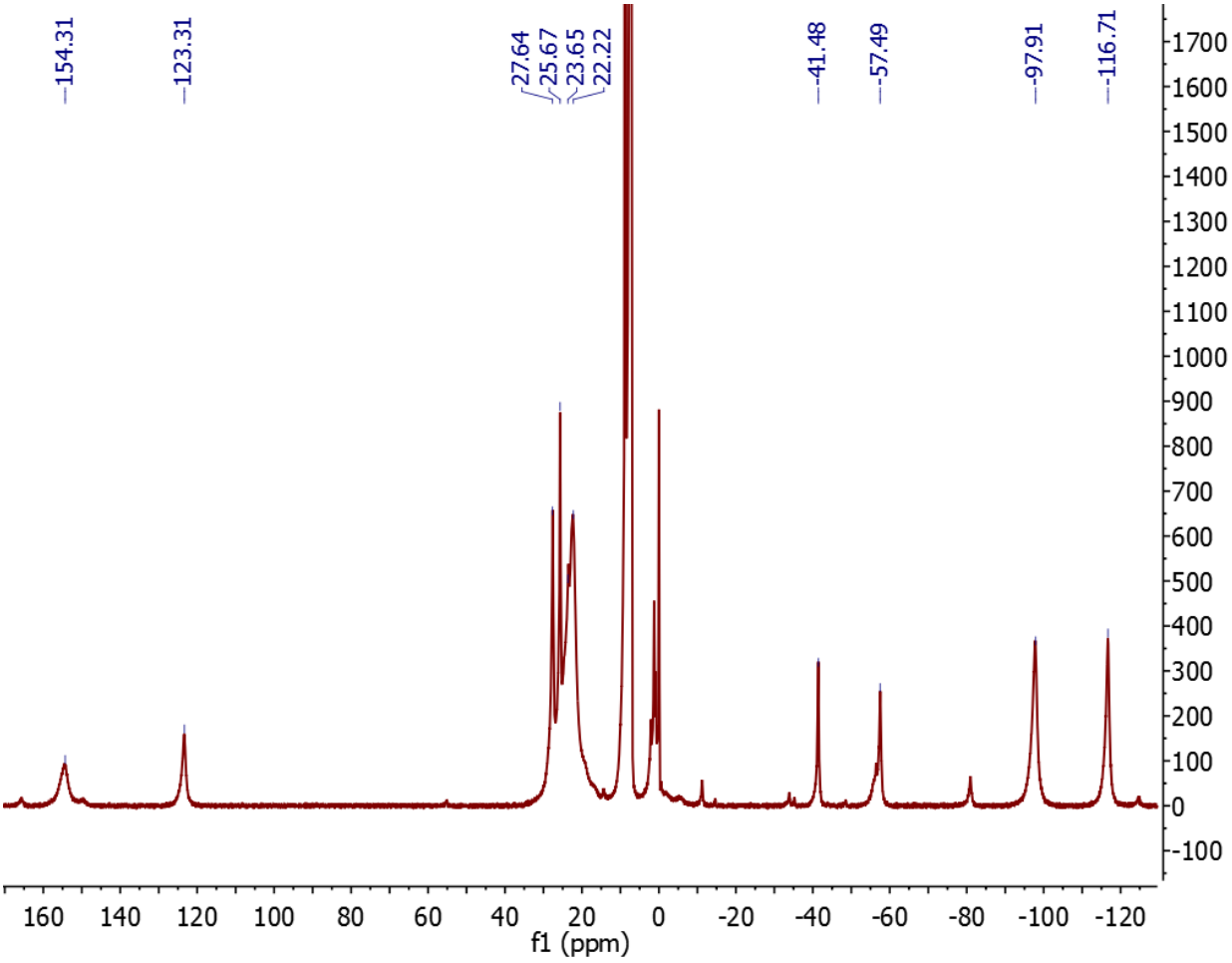

Figure S5. The ^{1}H NMR spectrum of $L^{Me,Me,Me}Fe(C_6H_6)$ dissolved in pyridine-d_5.

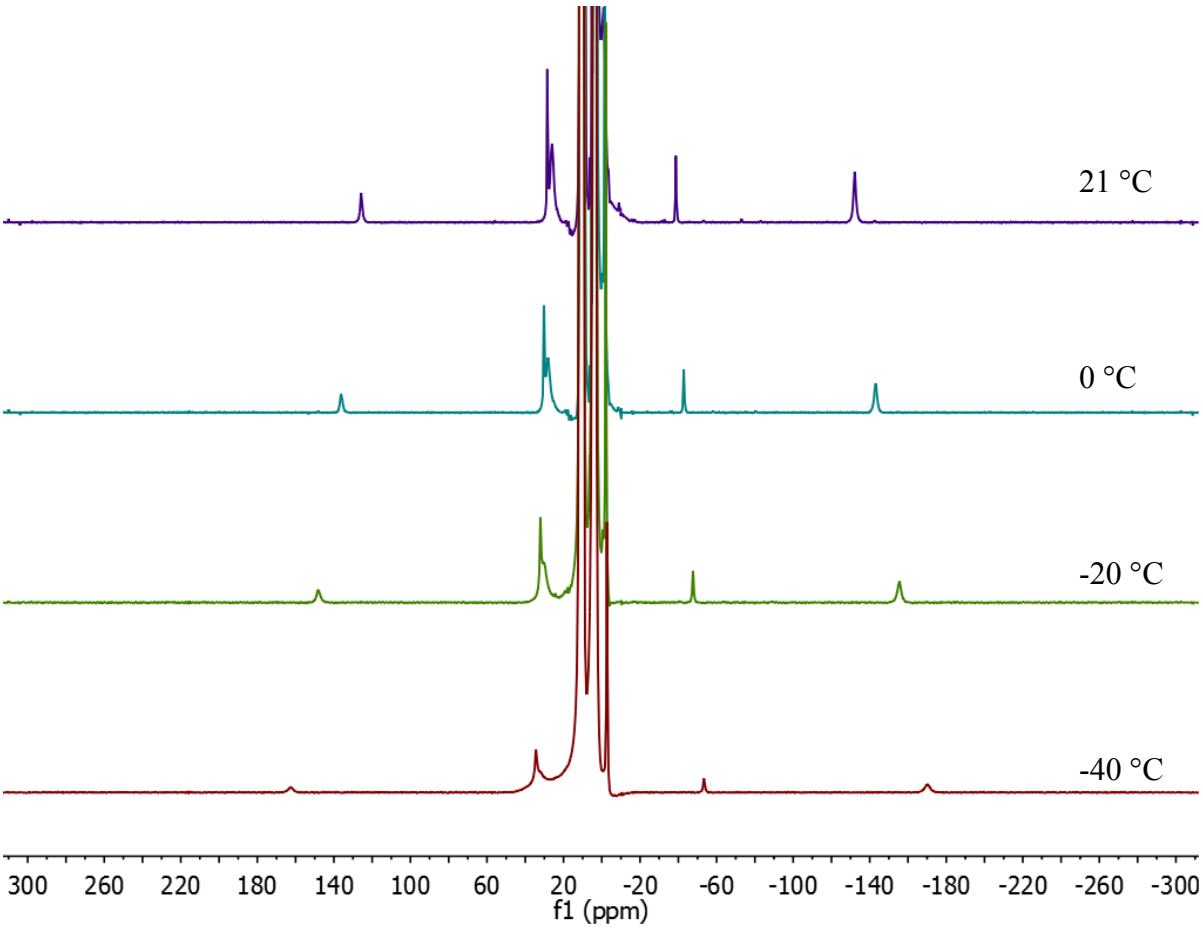

Figure S6. Variable temperature ^{1}H NMR spectra of LFe(C_6H_6) dissolved in *tert*-butylpyridine. Only one species is observed in solution at all temperatures utilized.

Dissolution of $L^{Me,Me,Me}Fe(\mu\text{-}C_6H_6)$ in *tert*-butylpyridine:

$L^{Me,Me,Me}Fe(C_6H_6)$ (9.6 mg, 0.021 mmol) was dissolved in 0.5052 g of tertbutylpyridine to give a green solution. A ^{1}H NMR spectrum was collected.

^{1}H NMR (tertbutylpyridine, 21.0 °C, 400 MHz): δ 125.6 (s, 3, γ-CH_3), 28.5 (s, 4H, meta-CH), 25.9 (s, 12H, ortho-CH_3), -38.7 (s, 2H, para-CH), -132.2 (s, 6H, β-CH_3).

^{1}H NMR (tertbutylpyridine, 0.0 °C, 400 MHz): δ 136.0 (s, 3, γ-CH_3), 30.2 (s, 4H, meta-CH), 28.0 (s, 12H, ortho-CH_3), -42.9 (s, 2H, para-CH), -143.2 (s, 6H, β-CH_3).

^{1}H NMR (tertbutylpyridine, -20.2 °C, 400 MHz): δ 147.9 (s, 3, γ-CH_3), 32.1 (s, 4H, meta-CH), 30.0 (s, 12H, ortho-CH_3), -47.8 (s, 2H, para-CH), -155.5 (s, 6H, β-CH_3).

^{1}H NMR (tertbutylpyridine, -40.1 °C, 400 MHz): δ 162.5 (s, 3, γ-CH_3), 34.4 (s, 4H, meta-CH), 33.0 (s, 12H, ortho-CH_3), -53.5 (s, 2H, para-CH), -170.1 (s, 6H, β-CH_3).

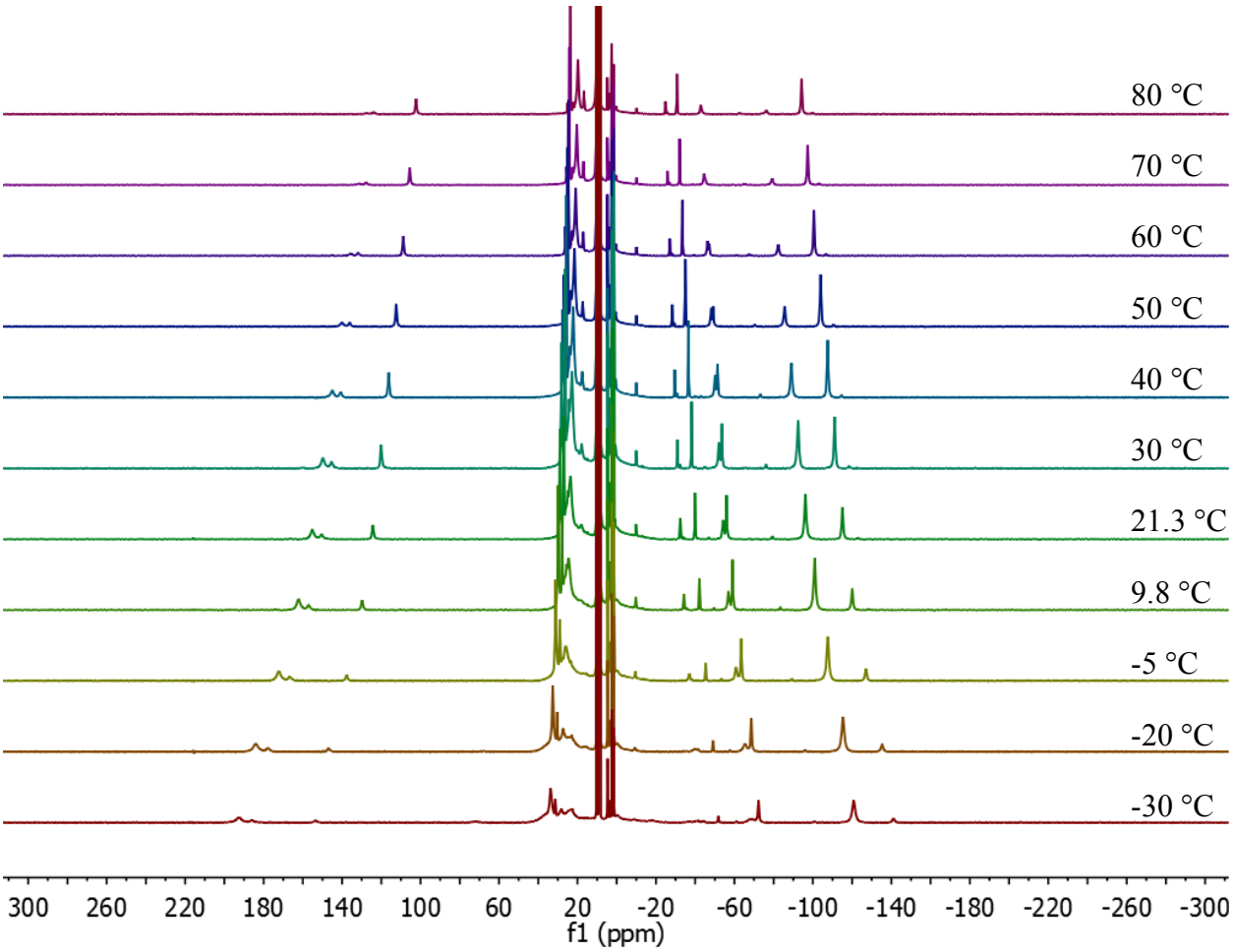

Figure S7. Variable temperature ^{1}H NMR spectra of LFe(Py)(μ-$C_{10}H_{10}N_2$)(Py)FeL (**1$_1$**) in pyridine-d_5.

Variable temperature analysis of LFe(Py)(μ-$C_{10}H_{10}N_2$)(Py)FeL (1$_1$) in Pyridine-d_5:

LFe(Py)(μ-$C_{10}H_{10}N_2$)(Py)FeL (**1$_1$**) (14.0 mg, 0.032 mmol) was dissolved in 0.5597 g (571.1 μL) of pyridine-d_5 to give a red solution. A ^{1}H NMR spectrum was collected.

^{1}H NMR (pyridine-d_5, 80 °C, 400 MHz): δ 126.9 (s, 3H, γ-CH_3, **1$_1$**), 102.3 (s, 3H, γ-CH_3, **1$_2$**), 23.7 (s, 4H, meta-CH, **1$_1$**), 19.7 (s, 12H, ortho-CH_3, **1$_1$**), -30.8 (s, 2H, para-CH, **1$_1$**), -42. 9 (s, 2H, para-CH, **1$_2$**), -76.4 (s, 6H, β-CH_3, **1$_2$**), -94.3 (s, 6H, β-CH_3, **1$_1$**).

^{1}H NMR (pyridine-d_5, 70 °C, 400 MHz): δ 131.6 (s, 3H, γ-CH_3, **1$_1$**), 105.5 (s, 3H, γ-CH_3, **1$_2$**), 24.1 (s, 4H, meta-CH, **1$_1$**), 20.3 (s, 12H, ortho-CH_3, **1$_1$**), -32.1 (s, 2H, para-CH, **1$_1$**), -44. 5 (s, 2H, para-CH, **1$_2$**), -79.2 (s, 6H, β-CH_3, **1$_2$**), -97.3 (s, 6H, β-CH_3, **1$_1$**).

^{1}H NMR (pyridine-d_5, 60 °C, 400 MHz): δ 135.7 (s, 3H, γ-CH_3, **1$_1$**), 108.8 (s, 3H, γ-CH_3, **1$_2$**), 26.2 (s, 4H, meta-CH, **1$_2$**), 24.7 (s, 4H, meta-CH, **1$_1$**), 23.0 (s, 12H, ortho-CH_3, **1$_2$**), 21.0 (s, 12H,

ortho-CH_3, **1_1**), -33.5 (s, 2H, para-CH, **1_1**), -46. 3 (s, 2H, para-CH, **1_2**), -82.3 (s, 6H, β-CH_3, **1_2**), -100.5 (s, 6H, β-CH_3, **1_1**).

NMR (pyridine-d_5, 50 °C, 400 MHz): δ 140.2 (s, 3H, γ-CH_3, **1_1**), 112.4 (s, 3H, γ-CH_3, **1_2**), 26.8 (s, 4H, meta-CH, **1_2**), 25.2 (s, 4H, meta-CH, **1_1**), 23.4 (s, 12H, ortho-CH_3, **1_2**), 21.5 (s, 12H, ortho-CH_3, **1_1**), -35.0 (s, 2H, para-CH, **1_1**), -49.2 (s, 2H, para-CH, **1_2**), -85.8 (s, 6H, β-CH_3, **1_2**), -104.0 (s, 6H, β-CH_3, **1_1**).

NMR (pyridine-d_5, 40 °C, 400 MHz): δ 144.9 (s, 3H, γ-CH_3, **1_1**), 116.2 (s, 3H, γ-CH_3, **1_2**), 27.5 (s, 4H, meta-CH, **1_2**), 25.8 (s, 4H, meta-CH, **1_1**), 23.9 (s, 12H, ortho-CH_3, **1_2**), 22.2 (s, 12H, ortho-CH_3, **1_1**), -36.6 (s, 2H, para-CH, **1_1**), -50.1 (s, 2H, para-CH, **1_2**), -89.1 (s, 6H, β-CH_3, **1_2**), -107.5 (s, 6H, β-CH_3, **1_1**).

NMR (pyridine-d_5, 30 °C, 400 MHz): δ 149.9 (s, 3H, γ-CH_3, **1_1**), 120.0 (s, 3H, γ-CH_3, **1_2**), 28.2 (s, 4H, meta-CH, **1_2**), 26.3 (s, 4H, meta-CH, **1_1**), 24.3 (s, 12H, ortho-CH_3, **1_2**), 22.7 (s, 12H, ortho-CH_3, **1_1**), -38.2 (s, 2H, para-CH, **1_1**), -53.6 (s, 2H, para-CH, **1_2**), -92.6 (s, 6H, β-CH_3, **1_2**), -111.2 (s, 6H, β-CH_3, **1_1**).

NMR (pyridine-d_5, 21.3 °C, 400 MHz): δ 155.3 (s, 3H, γ-CH_3, **1_1**), 124.5 (s, 3H, γ-CH_3, **1_2**), 28.9 (s, 4H, meta-CH, **1_2**), 27.0 (s, 4H, meta-CH, **1_1**), 24.8 (s, 12H, ortho-CH_3, **1_2**), 23.5 (s, 12H, ortho-CH_3, **1_1**), -39.9 (s, 2H, para-CH, **1_1**), -56.0 (s, 2H, para-CH, **1_2**), -96.3 (s, 6H, β-CH_3, **1_2**), -115.1 (s, 6H, β-CH_3, **1_1**).

NMR (pyridine-d_5, 9.8 °C, 400 MHz): δ 162.1 (s, 3H, γ-CH_3, **1_1**), 129.8 (s, 3H, γ-CH_3, **1_2**), 29.8 (s, 4H, meta-CH, **1_2**), 27.8 (s, 4H, meta-CH, **1_1**), 25.5 (s, 12H, ortho-CH_3, **1_2**), 24.4 (s, 12H, ortho-CH_3, **1_1**), -42.2 (s, 2H, para-CH, **1_1**), -59.1 (s, 2H, para-CH, **1_2**), -101.0 (s, 6H, β-CH_3, **1_2**), -120.2 (s, 6H, β-CH_3, **1_1**).

NMR (pyridine-d_5, -5.0 °C, 400 MHz): δ 172.2 (s, 3H, γ-CH_3, **1_1**), 137.5 (s, 3H, γ-CH_3, **1_2**), 31.1 (s, 4H, meta-CH, **1_2**), 29.0 (s, 4H, meta-CH, **1_1**), 27.8 (s, 12H, ortho-CH_3, **1_2**), 25.6 (s, 12H, ortho-CH_3, **1_1**), -45.4 (s, 2H, para-CH, **1_1**), -63.5 (s, 2H, para-CH, **1_2**), -107.6 (s, 6H, β-CH_3, **1_2**), -127.2 (s, 6H, β-CH_3, **1_1**).

NMR (pyridine-d_5, -20.0 °C, 400 MHz): δ 183.8 (s, 3H, γ-CH_3, **1_1**), 146.8 (s, 3H, γ-CH_3, **1_2**), 32.6 (s, 4H, meta-CH, **1_2**), 30.3 (s, 4H, meta-CH, **1_1**), 27.3 (s, 12H, ortho-CH_3, **1_2**), 24.1 (s, 12H, ortho-CH_3, **1_1**), -49.1 (s, 2H, para-CH, **1_1**), -68.7 (s, 2H, para-CH, **1_2**), -115.4 (s, 6H, β-CH_3, **1_2**), -135.4 (s, 6H, β-CH_3, **1_1**).

NMR (pyridine-d_5, -30.0 °C, 400 MHz): δ 192.2 (s, 3H, γ-CH_3, **1_1**), 153.4 (s, 3H, γ-CH_3, **1_2**), 34.3 (s, 4H, meta-CH, **1_2**), 31.3 (s, 4H, meta-CH, **1_1**), 28.0 (s, 12H, ortho-CH_3, **1_2**), 22.6 (s, 12H, ortho-CH_3, **1_1**), -51.8 (s, 2H, para-CH, **1_1**), -72.4 (s, 2H, para-CH, **1_2**), -121.0 (s, 6H, β-CH_3, **1_2**), -141.1 (s, 6H, β-CH_3, **1_1**).

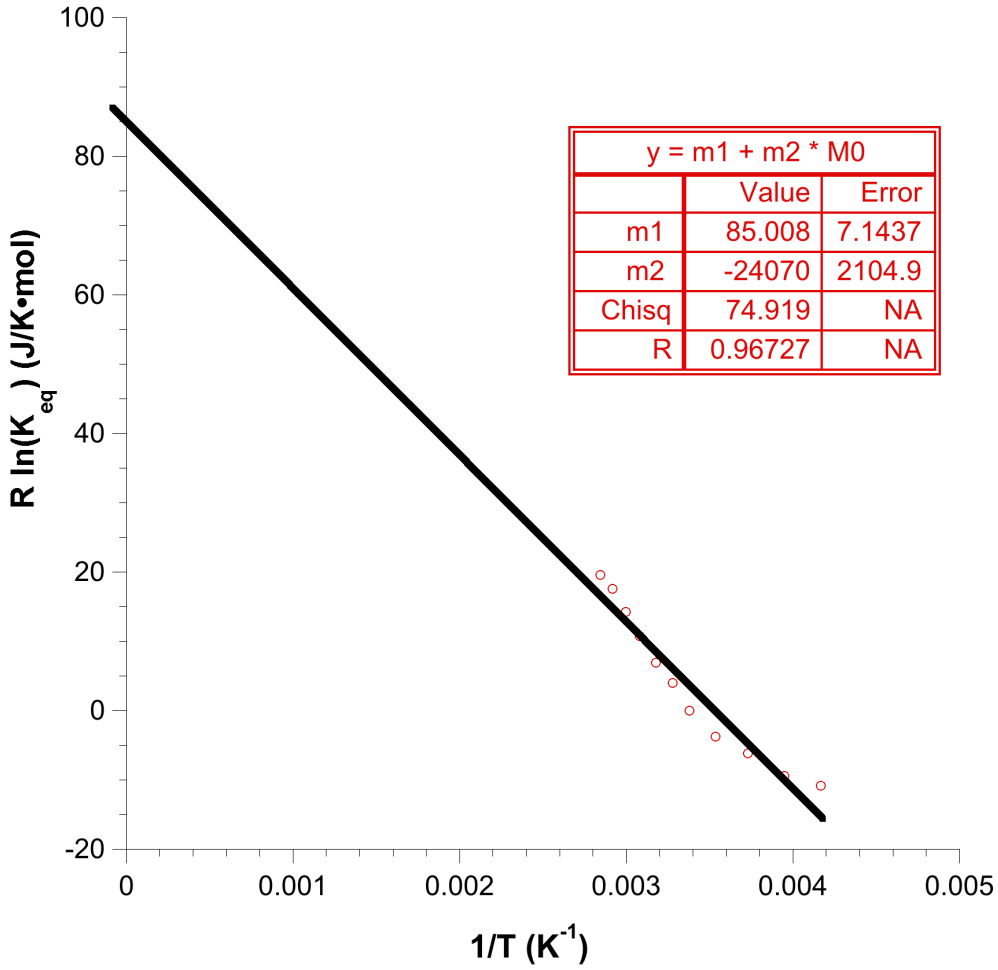

Figure S8. Plot of the integration ratios of $\mathbf{1_1}$ and $\mathbf{1_2}$ as a function of temperature to determine thermodynamic parameters for the equilibrium. This yields thermodynamic parameters $\Delta H°$ = 24 kJ/mol and $\Delta S°$ = 85 J/mol•K for the conversion of $\mathbf{1_2}$ to $\mathbf{1_1}$. The values in the text are given as the other direction of the equilibrium, to match the direction given in Scheme 2.

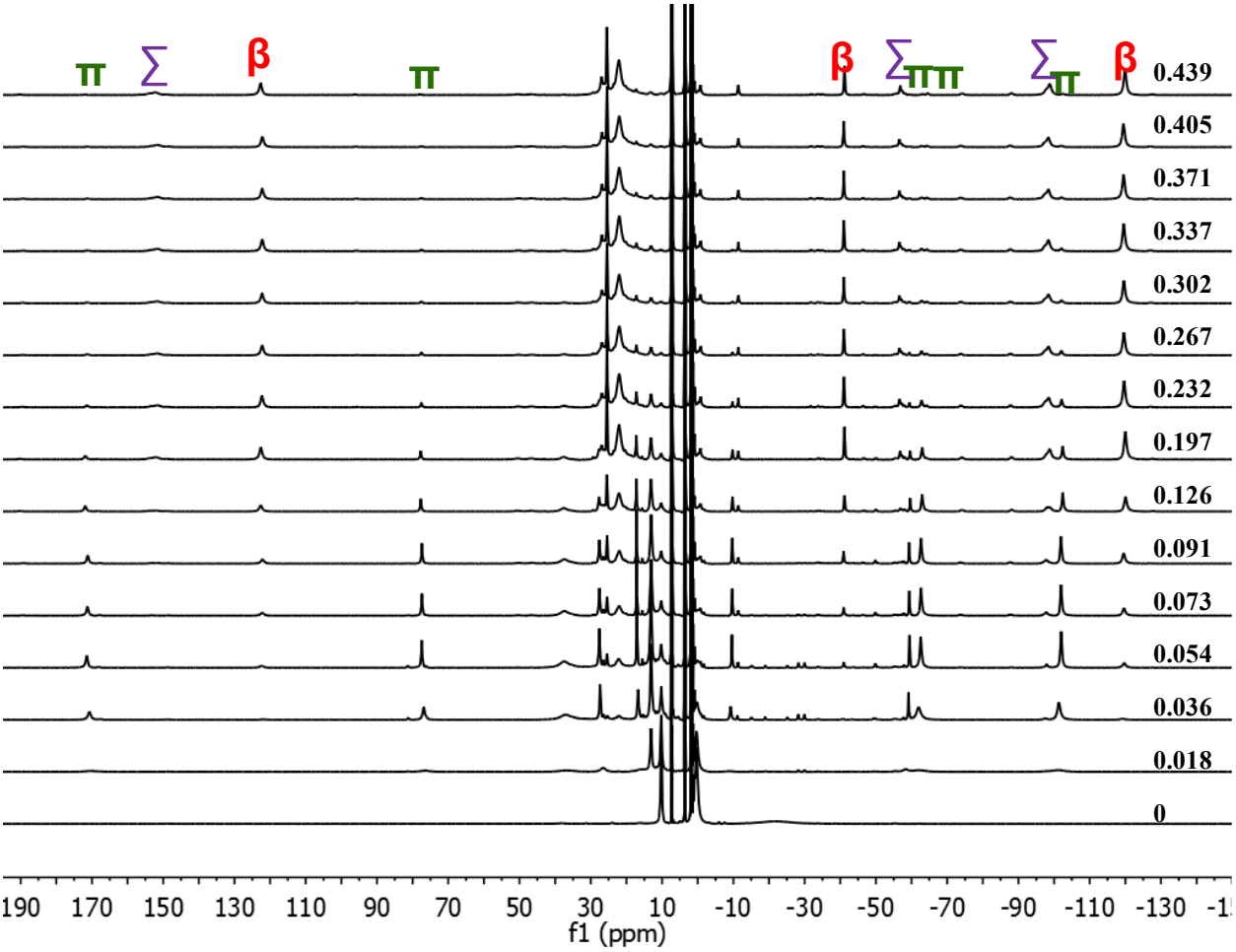

Figure S9a. Titration of pyridine-d_5 into a solution of LFe(C_6H_6). Numbers on the right indicate pyridine concentration in M. (β) indicates complex $\mathbf{1_1}$, (∑) indicates complex $\mathbf{1_2}$, (π) indicates complex **2**, and (Δ) indicates LFe(C_6H_6).

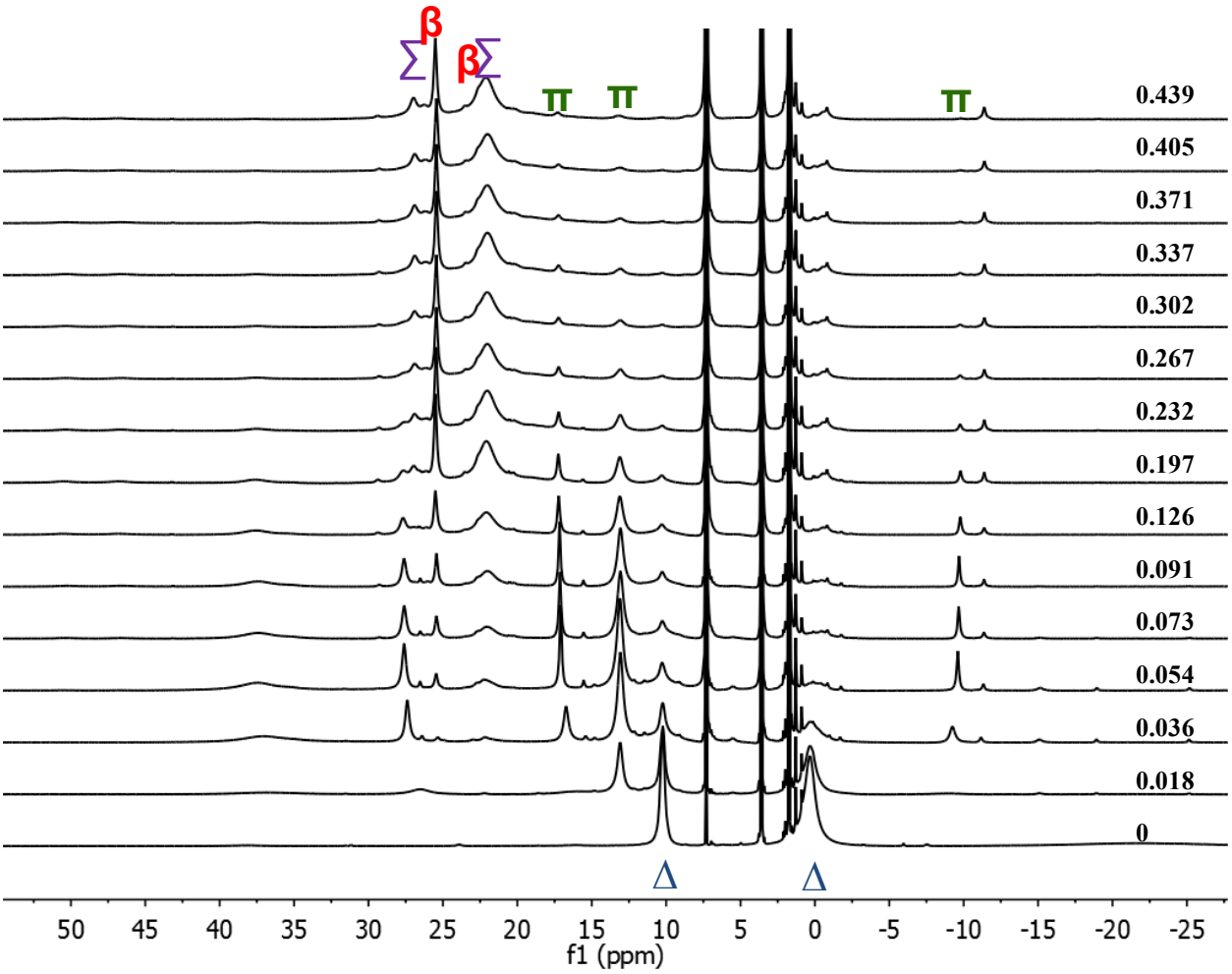

Figure S9b. Titration of pyridine-d_5 into a solution of LFe(C_6H_6). Numbers on the right indicate pyridine concentration in M. (β) indicates complex $\mathbf{1_1}$, (∑) indicates complex $\mathbf{1_2}$, (π) indicates complex **2**, and (Δ) indicates LFe(C_6H_6).

Titration of pyridine-d_5 into LFe(C_6H_6)

$L^{Me,Me,Me}Fe(C_6H_6)$ (12.1 mg, 0.0267 mmol) was dissolved in 0.639 mL of THF-d_8 to give a brown solution. A ^{1}H NMR spectrum was collected.

^{1}H NMR (THF-d_8, 21.0 °C, 400 MHz): δ 10.2, 0.3, -21.9 ppm. The peaks are difficult to assign in this S = ½ complex.

^{1}H NMR (0.018 M pyridine, THF-d_8, 21.0 °C, 400 MHz): δ 170.0 (s, 3H, γ-CH_3, **2**), 76.1 (s, 3H, γ-CH_3, **2**), 36.3 (br s, 6H, ortho-CH_3 or b-CH_3, **2**), 26.2 (s, 4H, meta-CH, **2**), 13.1 (s, 12H, ortho-CH_3, **2**), 10.2 (LFe(C_6H_6)), 0.31 (LFe(C_6H_6)), -8.8 (s, 2H, para-CH, **2**), -61.6 (s, 2H, para-CH, **2**), -101.5 (s, 6H, β-CH_3, **2**).

^{1}H NMR (0.036 M pyridine, THF-d_8, 21.0 °C, 400 MHz): δ170.7 (s, 3H, γ-CH_3, **2**),148.1 (s, 3H, γ-CH_3, $\mathbf{1_2}$), 121.6 (s, 3H, γ-CH_3, $\mathbf{1_1}$), 77.0 (s, 3H, γ-CH_3, **2**), 37.2 (br s, 6H, ortho-CH_3 or b-CH_3, **2**), 27.4 (s, 4H, meta-CH, **2**) , 25.4 (s, 4H, meta-CH, $\mathbf{1_2}$), 23.0 (s, 12H, ortho-CH_3, $\mathbf{1_1}$ & $\mathbf{1_2}$), 16.7 (s, 4H, meta-CH, **2**), 13.1 (s, 12H, ortho-CH_3, **2**), 10.2 (LFe(C_6H_6)), -9.3 (s, 2H, para-CH, **2**), -40.8 (s, 2H, para-CH. $\mathbf{1_1}$), -55.4 (s, 2H, para-CH, $\mathbf{1_2}$), -59.2 (s, 2H, para-CH, **2**), -62.0 (s, 6H, β-CH_3, **2**), -97.7 (s, 6H, β-CH_3, $\mathbf{1_2}$), -101.3 (s, 6H, β-CH_3, **2**), -119.0 (s, 6H, β-CH_3, $\mathbf{1_1}$).

^{1}H NMR (0.054 M pyridine, THF-d_8, 21.0 °C, 400 MHz): δ171.4 (s, 3H, γ-CH_3, **2**),148.7 (s, 3H, γ-CH_3, $\mathbf{1_2}$), 122.4 (s, 3H, γ-CH_3, $\mathbf{1_1}$), 77.4 (s, 3H, γ-CH_3, **2**), 37.4 (br s, 6H, ortho-CH_3 or b-CH_3, **2**), 27.6 (s, 4H, meta-CH, **2**) , 25.5 (s, 4H, meta-CH, $\mathbf{1_2}$), 22.2 (s, 12H, ortho-CH_3, $\mathbf{1_1}$ & $\mathbf{1_2}$), 17.1 (s, 4H, meta-CH, **2**), 13.1 (s, 12H, ortho-CH_3, **2**), 10.3 (LFe(C_6H_6)), -9.6 (s, 2H, para-CH, **2**), -41.0 (s, 2H, para-CH. $\mathbf{1_1}$), -55.6 (s, 2H, para-CH, $\mathbf{1_2}$), -59.4 (s, 2H, para-CH, **2**), -62.6 (s, 6H, β-CH_3, **2**), -97.9 (s, 6H, β-CH_3, $\mathbf{1_2}$), -102.0 (s, 6H, β-CH_3, **2**), -119.7 (s, 6H, β-CH_3, $\mathbf{1_1}$).

^{1}H NMR (0.073 M pyridine, THF-d_8, 21.0 °C, 400 MHz): δ171.2 (s, 3H, γ-CH_3, **2**),148.2 (s, 3H, γ-CH_3, $\mathbf{1_2}$), 122.2 (s, 3H, γ-CH_3, $\mathbf{1_1}$), 77.4 (s, 3H, γ-CH_3, **2**), 37.0 (br s, 6H, ortho-CH_3 or b-CH_3, **2**), 27.6 (s, 4H, meta-CH, **2**) , 25.4 (s, 4H, meta-CH, $\mathbf{1_2}$), 22.0 (s, 12H, ortho-CH_3, $\mathbf{1_1}$ & $\mathbf{1_2}$), 17.1 (s, 4H, meta-CH, **2**), 13.1 (s, 12H, ortho-CH_3, **2**), 10.2 (LFe(C_6H_6)), -9.7 (s, 2H, para-CH, **2**), -41.0 (s, 2H, para-CH. $\mathbf{1_1}$), -55.3 (s, 2H, para-CH, $\mathbf{1_2}$), -59.4 (s, 2H, para-CH, **2**), -62.7 (s, 6H, β-CH_3, **2**), -97.8 (s, 6H, β-CH_3, $\mathbf{1_2}$), -102.0 (s, 6H, β-CH_3, **2**), -119.7 (s, 6H, β-CH_3, $\mathbf{1_1}$).

^{1}H NMR (0.091 M pyridine, THF-d_8, 21.0 °C, 400 MHz): δ171.1 (s, 3H, γ-CH_3, **2**),151.9 (s, 3H, γ-CH_3, $\mathbf{1_2}$), 122.2 (s, 3H, γ-CH_3, $\mathbf{1_1}$), 77.4 (s, 3H, γ-CH_3, **2**), 37.4 (br s, 6H, ortho-CH_3 or b-CH_3, **2**), 27.6 (s, 4H, meta-CH, **2**) , 25.4 (s, 4H, meta-CH, $\mathbf{1_2}$), 21.9 (s, 12H, ortho-CH_3, $\mathbf{1_1}$ & $\mathbf{1_2}$), 17.2 (s, 4H, meta-CH, **2**), 13.1 (s, 12H, ortho-CH_3, **2**), 10.3 (LFe(C_6H_6)), -9.7 (s, 2H, para-CH, **2**), -41.0 (s, 2H, para-CH. $\mathbf{1_1}$), -55.2 (s, 2H, para-CH, $\mathbf{1_2}$), -59.3 (s, 2H, para-CH, **2**), -62.7 (s, 6H, β-CH_3, **2**), -97.7 (s, 6H, β-CH_3, $\mathbf{1_2}$), -101.9 (s, 6H, β-CH_3, **2**), -119.6 (s, 6H, β-CH_3, $\mathbf{1_1}$).

^{1}H NMR (0.126 M pyridine, THF-d_8, 21.0 °C, 400 MHz): δ171.9 (s, 3H, γ-CH_3, **2**),151.1 (s, 3H, γ-CH_3, $\mathbf{1_2}$), 122.5 (s, 3H, γ-CH_3, $\mathbf{1_1}$), 77.7 (s, 3H, γ-CH_3, **2**), 37.3 (br s, 6H, ortho-CH_3 or b-CH_3, **2**), 27.7 (s, 4H, meta-CH, **2**) , 25.5 (s, 4H, meta-CH, $\mathbf{1_2}$), 22.0 (s, 12H, ortho-CH_3, $\mathbf{1_1}$ & $\mathbf{1_2}$), 17.2 (s, 4H, meta-CH, **2**), 13.1 (s, 12H, ortho-CH_3, **2**), 10.3 (LFe(C_6H_6)), -9.8 (s, 2H, para-CH, **2**), -41.2 (s, 2H, para-CH. $\mathbf{1_1}$), -55.7 (s, 2H, para-CH, $\mathbf{1_2}$), -59.6 (s, 2H, para-CH, **2**), -63.0 (s, 6H, β-CH_3, **2**), -98.2 (s, 6H, β-CH_3, $\mathbf{1_2}$), -102.4 (s, 6H, β-CH_3, **2**), -120.1 (s, 6H, β-CH_3, $\mathbf{1_1}$).

^{1}H NMR (0.197 M pyridine, THF-d_8, 21.0 °C, 400 MHz): δ171.8 (s, 3H, γ-CH_3, **2**),151.9 (s, 3H, γ-CH_3, $\mathbf{1_2}$), 122.5 (s, 3H, γ-CH_3, $\mathbf{1_1}$), 77.7 (s, 3H, γ-CH_3, **2**), 37.4 (br s, 6H, ortho-CH_3 or b-CH_3, **2**), 27.0 (s, 4H, meta-CH, **2**) , 25.5 (s, 4H, meta-CH, $\mathbf{1_2}$), 22.0 (s, 12H, ortho-CH_3, $\mathbf{1_1}$ & $\mathbf{1_2}$), 17.2 (s, 4H, meta-CH, **2**), 13.1 (s, 12H, ortho-CH_3, **2**), 10.2 (LFe(C_6H_6)), -9.8 (s, 2H, para-CH, **2**), -41.2 (s, 2H, para-CH. $\mathbf{1_1}$), -56.8 (s, 2H, para-CH, $\mathbf{1_2}$), -59.6 (s, 2H, para-CH, **2**), -63.0 (s, 6H, β-CH_3, **2**), -98.7 (s, 6H, β-CH_3, $\mathbf{1_2}$), -102.4 (s, 6H, β-CH_3, **2**), -120.0 (s, 6H, β-CH_3, $\mathbf{1_1}$).

^{1}H NMR (0.232 M pyridine, THF-d_8, 21.0 °C, 400 MHz): δ171.5 (s, 3H, γ-CH_3, **2**),151.4 (s, 3H, γ-CH_3, $\mathbf{1_2}$), 122.2 (s, 3H, γ-CH_3, $\mathbf{1_1}$), 77.5 (s, 3H, γ-CH_3, **2**), 37.5 (br s, 6H, ortho-CH_3 or b-CH_3, **2**), 26.9 (s, 4H, meta-CH, **2**) , 25.5 (s, 4H, meta-CH, $\mathbf{1_2}$), 21.9 (s, 12H, ortho-CH_3, $\mathbf{1_1}$ & $\mathbf{1_2}$), 17.2 (s, 4H, meta-CH, **2**), 13.1 (s, 12H, ortho-CH_3, **2**), 10.2 (LFe(C_6H_6)), -9.7 (s, 2H, para-CH, **2**), -41.0 (s, 2H, para-CH. $\mathbf{1_1}$), -56.6 (s, 2H, para-CH, $\mathbf{1_2}$), -59.4 (s, 2H, para-CH, **2**), -62.9 (s, 6H, β-CH_3, **2**), -98.6 (s, 6H, β-CH_3, $\mathbf{1_2}$), -102.2 (s, 6H, β-CH_3, **2**), -119.6 (s, 6H, β-CH_3, $\mathbf{1_1}$).

^{1}H NMR (0.267 M pyridine, THF-d_8, 21.0 °C, 400 MHz): δ171.3 (s, 3H, γ-CH_3, **2**),151.5 (s, 3H, γ-CH_3, $\mathbf{1_2}$), 122.3 (s, 3H, γ-CH_3, $\mathbf{1_1}$), 77.5 (s, 3H, γ-CH_3, **2**), 26.9 (s, 4H, meta-CH, **2**) , 25.4 (s, 4H, meta-CH, $\mathbf{1_2}$), 21.9 (s, 12H, ortho-CH_3, $\mathbf{1_1}$ & $\mathbf{1_2}$), 17.2 (s, 4H, meta-CH, **2**), 13.0 (s, 12H, ortho-CH_3, **2**), 10.2 (LFe(C_6H_6)), -9.8 (s, 2H, para-CH, **2**), -41.0 (s, 2H, para-CH. $\mathbf{1_1}$), -56.6 (s, 2H, para-CH, $\mathbf{1_2}$), -59.4 (s, 2H, para-CH, **2**), -62.9 (s, 6H, β-CH_3, **2**), -98.5 (s, 6H, β-CH_3, $\mathbf{1_2}$), -102.1 (s, 6H, β-CH_3, **2**), -119.6 (s, 6H, β-CH_3, $\mathbf{1_1}$).

^{1}H NMR (0.302 M pyridine, THF-d_8, 21.0 °C, 400 MHz): δ171.3 (s, 3H, γ-CH_3, **2**),151.6 (s, 3H, γ-CH_3, $\mathbf{1_2}$), 122.2 (s, 3H, γ-CH_3, $\mathbf{1_1}$), 77.5 (s, 3H, γ-CH_3, **2**), 26.9 (s, 4H, meta-CH, **2**) , 25.5 (s, 4H, meta-CH, $\mathbf{1_2}$), 22.0 (s, 12H, ortho-CH_3, $\mathbf{1_1}$ & $\mathbf{1_2}$), 17.2 (s, 4H, meta-CH, **2**), 13.1 (s, 12H, ortho-CH_3, **2**), 10.2 (LFe(C_6H_6)), -9.8 (s, 2H, para-CH, **2**), -41.0 (s, 2H, para-CH. $\mathbf{1_1}$), -56.6 (s, 2H, para-CH, $\mathbf{1_2}$), -98.5 (s, 6H, β-CH_3, $\mathbf{1_2}$), -102.1 (s, 6H, β-CH_3, **2**), -119.5 (s, 6H, β-CH_3, $\mathbf{1_1}$).

^{1}H NMR (0.337 M pyridine, THF-d_8, 21.0 °C, 400 MHz): δ151.2 (s, 3H, γ-CH_3, $\mathbf{1_2}$), 122.3 (s, 3H, γ-CH_3, $\mathbf{1_1}$), 26.9 (s, 4H, meta-CH, **2**) , 25.4 (s, 4H, meta-CH, $\mathbf{1_2}$), 21.9 (s, 12H, ortho-CH_3, $\mathbf{1_1}$ & $\mathbf{1_2}$), -41.0 (s, 2H, para-CH. $\mathbf{1_1}$), -56.6 (s, 2H, para-CH, $\mathbf{1_2}$), -98.5 (s, 6H, β-CH_3, $\mathbf{1_2}$), -102.1 (s, 6H, β-CH_3, **2**), -119.6 (s, 6H, β-CH_3, $\mathbf{1_1}$).

^{1}H NMR (0.371 M pyridine, THF-d_8, 21.0 °C, 400 MHz): δ151.4 (s, 3H, γ-CH_3, $\mathbf{1_2}$), 122.2 (s, 3H, γ-CH_3, $\mathbf{1_1}$), 26.9 (s, 4H, meta-CH, **2**) , 25.5 (s, 4H, meta-CH, $\mathbf{1_2}$), 22.1 (s, 12H, ortho-CH_3, $\mathbf{1_1}$ & $\mathbf{1_2}$), -41.0 (s, 2H, para-CH. $\mathbf{1_1}$), -56.6 (s, 2H, para-CH, $\mathbf{1_2}$), -98.4 (s, 6H, β-CH_3, $\mathbf{1_2}$), -119.5 (s, 6H, β-CH_3, $\mathbf{1_1}$).

^{1}H NMR (0.405 M pyridine, THF-d_8, 21.0 °C, 400 MHz): δ151.9 (s, 3H, γ-CH_3, $\mathbf{1_2}$), 122.1 (s, 3H, γ-CH_3, $\mathbf{1_1}$), 25.4 (s, 4H, meta-CH, $\mathbf{1_2}$), 21.9 (s, 12H, ortho-CH_3, $\mathbf{1_1}$ & $\mathbf{1_2}$), -41.0 (s, 2H, para-CH. $\mathbf{1_1}$), -56.6 (s, 2H, para-CH, $\mathbf{1_2}$), -98.3 (s, 6H, β-CH_3, $\mathbf{1_2}$), -119.5 (s, 6H, β-CH_3, $\mathbf{1_1}$).

^{1}H NMR (0.439 M pyridine, THF-d_8, 21.0 °C, 400 MHz): δ152.4 (s, 3H, γ-CH_3, $\mathbf{1_2}$), 122.6 (s, 3H, γ-CH_3, $\mathbf{1_1}$), 25.5 (s, 4H, meta-CH, $\mathbf{1_2}$), 22.0 (s, 12H, ortho-CH_3, $\mathbf{1_1}$ & $\mathbf{1_2}$), -41.2 (s, 2H, para-CH. $\mathbf{1_1}$), -56.9 (s, 2H, para-CH, $\mathbf{1_2}$), -98.9 (s, 6H, β-CH_3, $\mathbf{1_2}$), -120.0 (s, 6H, β-CH_3, $\mathbf{1_1}$).

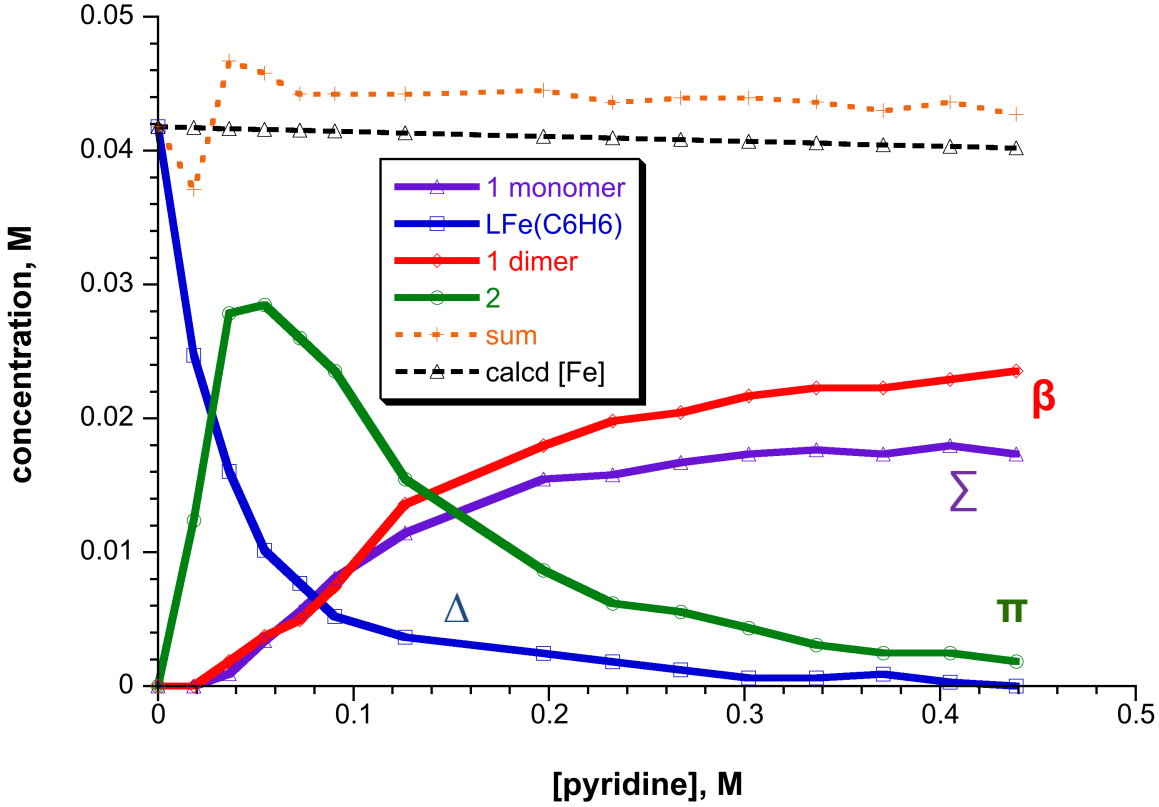

Figure S10. Graphical representation of the change in concentration of each species in solution from Figures S9a and S9b. (∑) indicates complex $\mathbf{1}_1$, (β) indicates complex $\mathbf{1}_2$, (π) indicates complex **2**, and (Δ) indicates LFe(C_6H_6). The gold dashed line gives the sum of the integrations, which is close to the total concentration expected from the amount of LFe(C_6H_6) originally added (dashed black line).

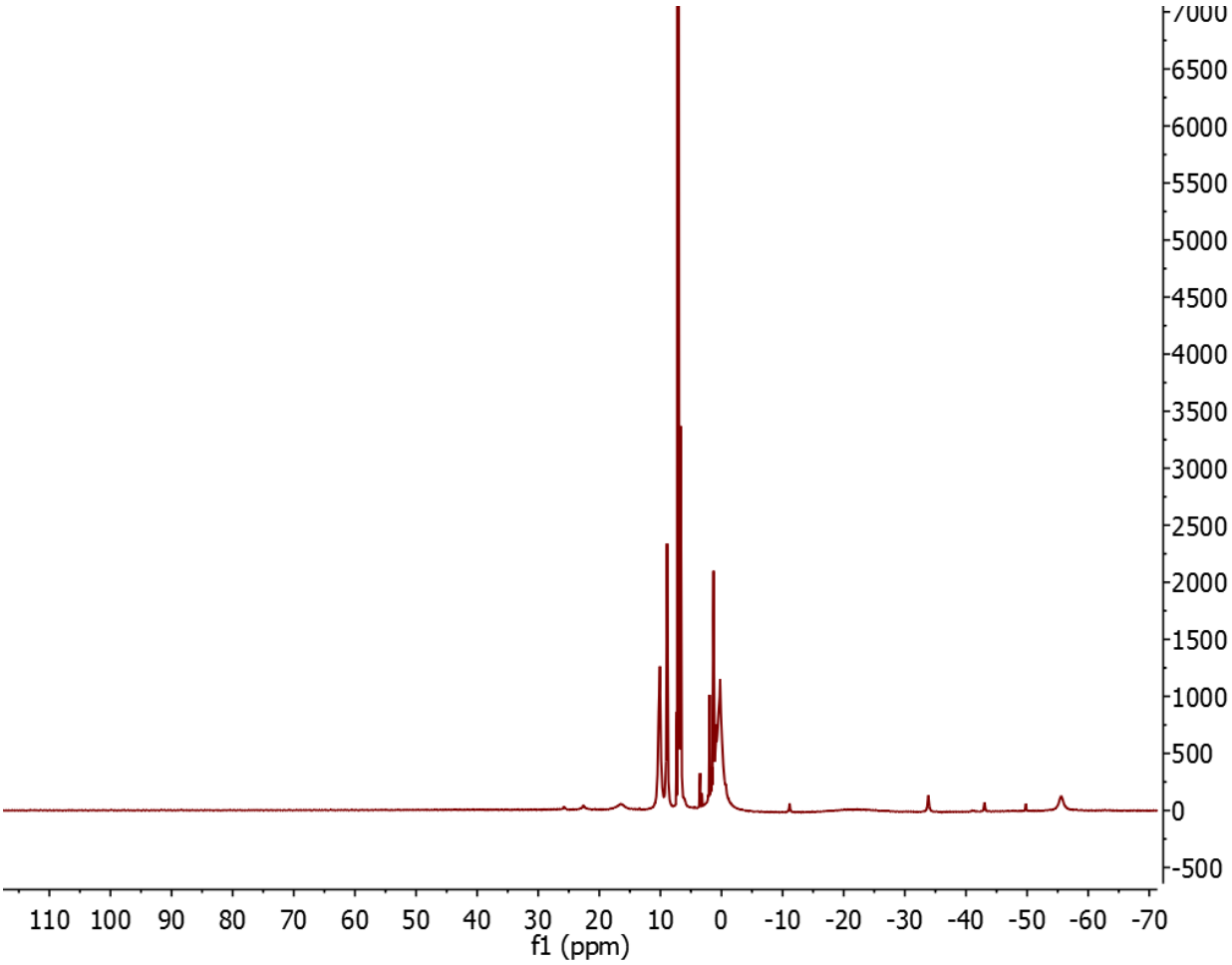

Figure S11. ^{1}H NMR spectrum of LFe(Py)($N_2C_{10}H_{10}$)(Py)FeL (**1$_2$**) dissolved in C_6D_6.

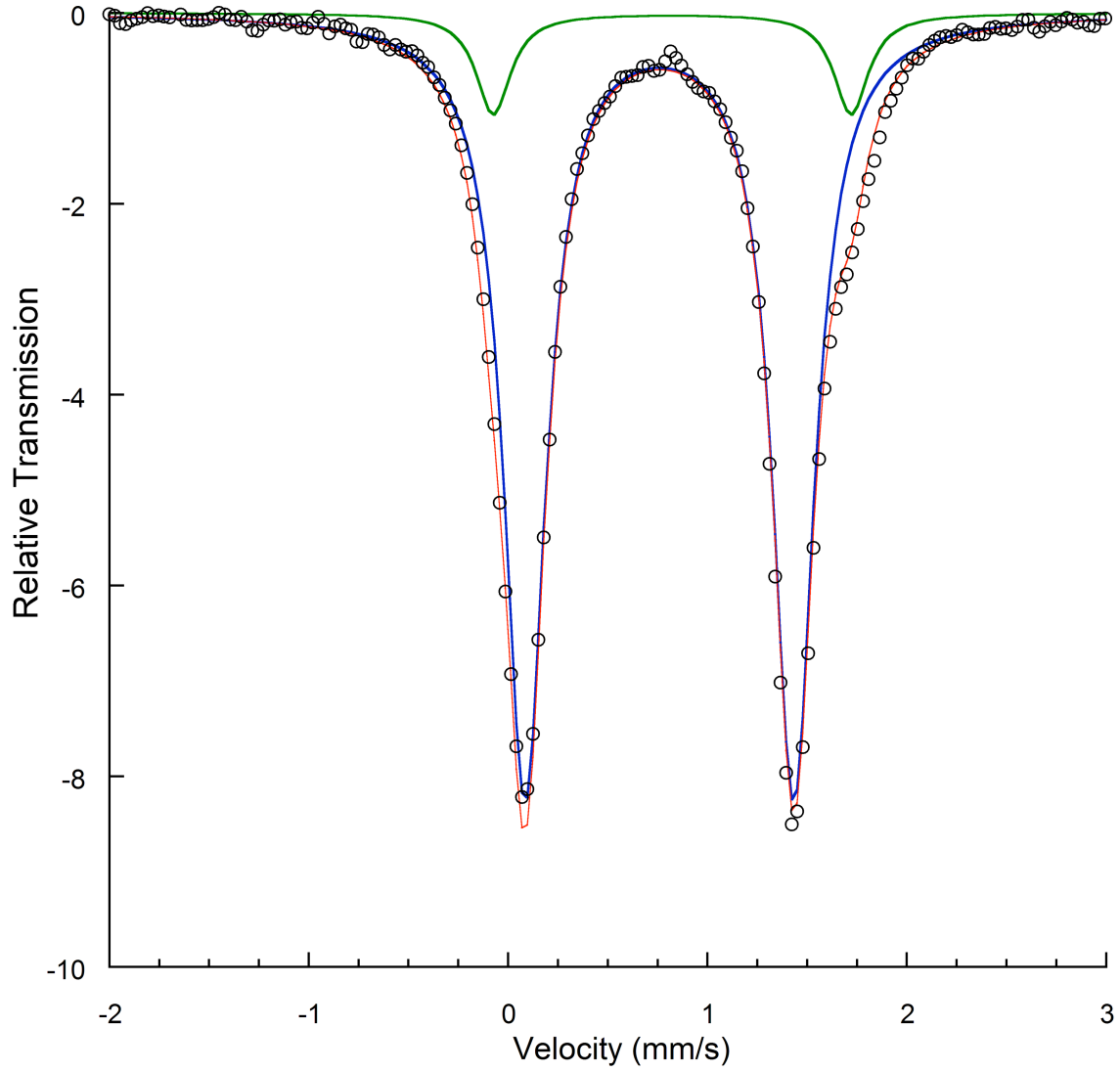

Figure S12. Solid state Mossbauer spectrum of $\mathbf{1_2}$ at 80 K. Major component: $\delta = 0.76$ mm/s; $|\Delta E_q| = 1.38$ mm/s; Gamma = 0.256; Relative Area = 91%. Minor component (impurity): $\delta = 0.82$ mm/s; $|\Delta E_q| = 1.79$ mm/s; Gamma = 0.209; Relative Area = 9%.

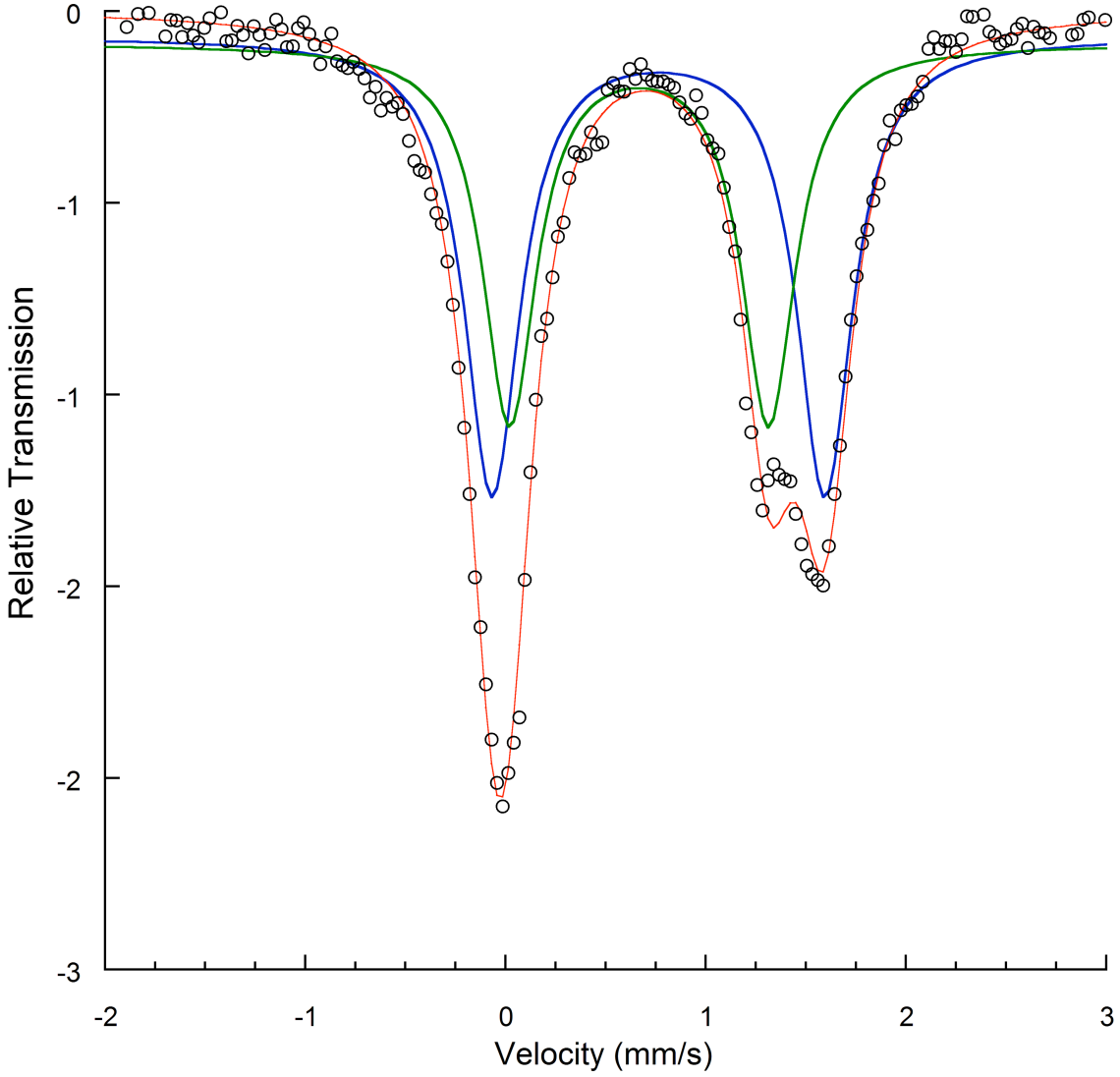

Figure S13. Solid state Mossbauer spectrum of **2** at 80 K. Major component: $\delta = 0.76$ mm/s; $|\Delta E_q| = 1.66$ mm/s; Gamma = 0.336; Relative Area = 55%. Minor component: $\delta = 0.67$ mm/s; $|\Delta E_q| = 1.29$ mm/s; Gamma = 0.323; Relative Area = 45%.

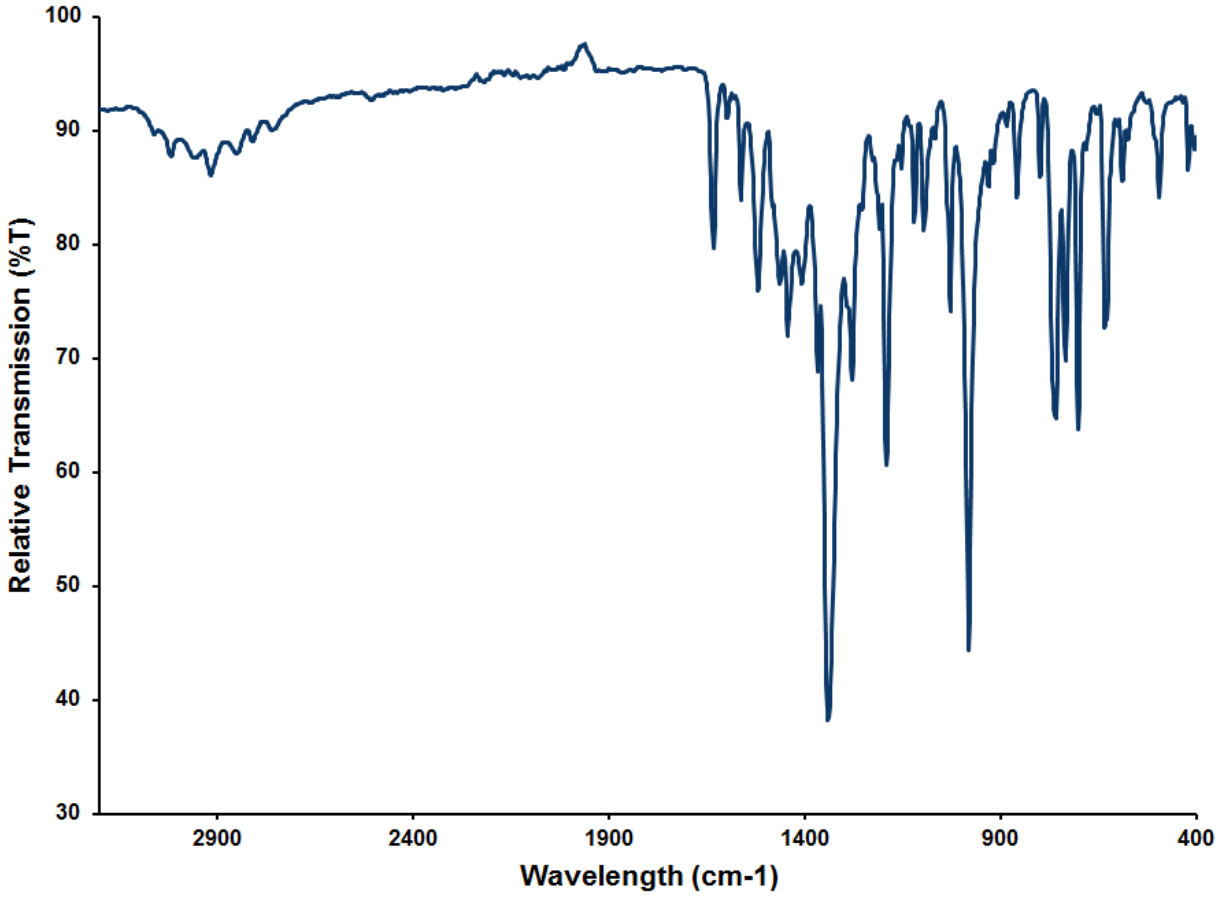

Figure S14. Solid state IR spectrum of $\mathbf{1_2}$ (neat).

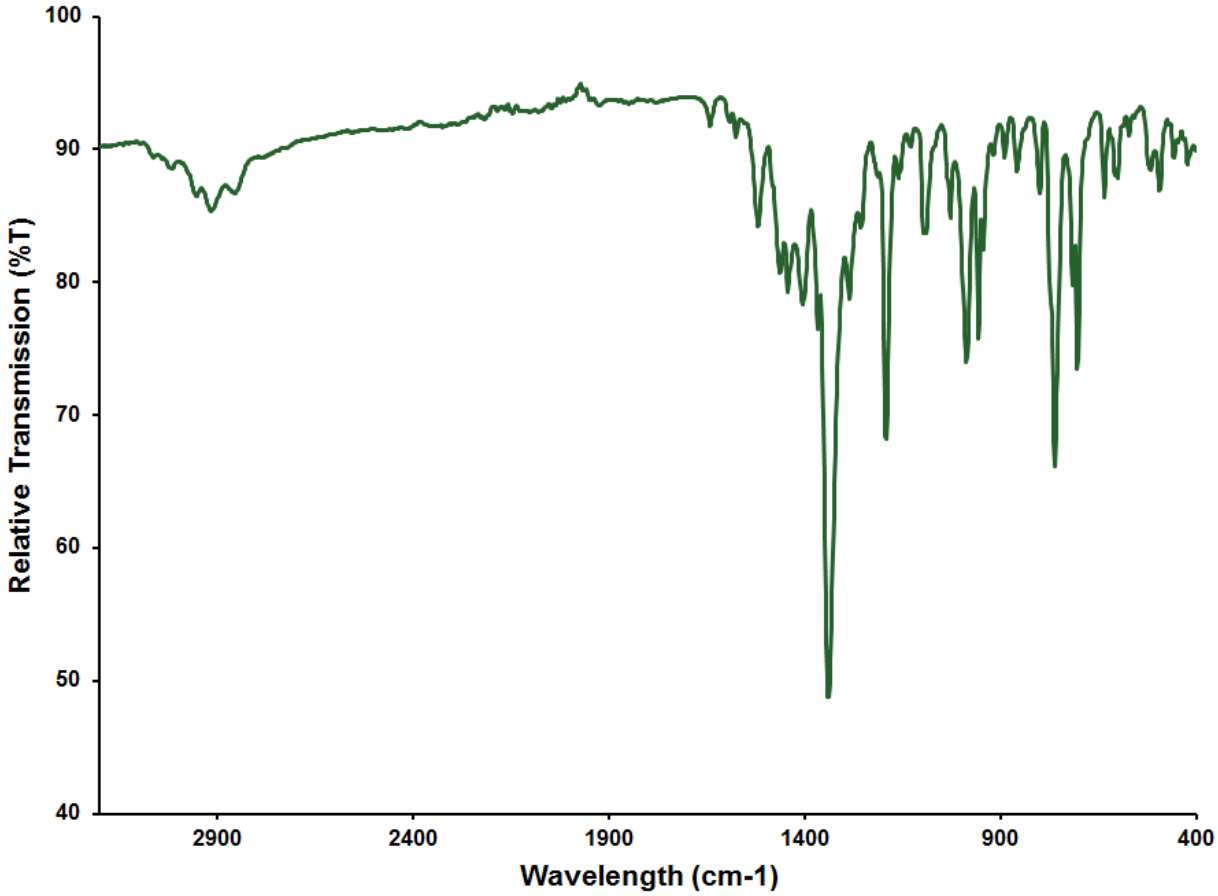

Figure S15. Solid state IR spectrum of **2** (neat).

Computations

We performed DFT calculations with the ORCA program package, version 3.0.1.[1] Calculations reported here employed the TPSSh functional.[2] The Ahlrichs triple-ζ-quality basis set with one set of polarization functions, TZVP, was used for all non-hydrogen atoms.[3] The smaller polarized Ahlrichs double-ζ-quality basis set, def2-SVP, was used on hydrogen atoms. No auxiliary basis set was used, because we desired to reproduce the conditions used in the literature correlation of isomer shifts to electron density on the Fe nucleus.[4] An empirical van der Waals correction was applied to the DFT energy (D3BJ).[5] The SCF calculations were tightly converged (TightSCF) with unrestricted spin (UKS), and relativistic effects (ZORA). The geometries used had all of the non-hydrogen atoms at the crystallographic positions, and the H positions were optimized in order to correct for the known systematic error in crystallographically determined X-H distances.[6]

For compound $\mathbf{1_2}$, we assumed two high-spin iron(II) sites. The calculations were repeated using the geometries of both C-C coupled dimers in the structure of $\mathbf{1_2}$. The calculated energies were somewhat different, but this is not surprising since the geometries were not optimized. The predicted Mössbauer parameters were very similar for the two inequivalent dimers (and for the two iron sites within each dimer), suggesting that the Mössbauer predictions are not sensitive to the small differences between the sites. Note that the calculations give predictions with a systematic error of ~0.14 mm/s lower than the experimental value. Preliminary calculations on the published system $(L'FePy)_2(\mu\text{-}C_{10}H_{10}N_2)$ also give a similar deviation. Others have also found systematic deviations of calculated isomer shifts of 0.10 to 0.15 mm/s to the low side in complexes of redox-active ligands.[7]

For compound **2**, we tested nonet, septet, quintet, triplet, and singlet states of the overall molecule. The septet state had the lowest energy, and the best agreement with the isomer shift. A broken-symmetry calculation with 4 unpaired α spins and 2 unpaired β spins gave calculated Mössbauer parameters the same (within 0.04 mm/s) as the septet. The 0.14 mm/s deviation of each isomer shift from experimental values is attributed to a systematic error in calculated isomer shifts in these complexes, as shown by analogous calculations on $(L'FePy)_2(\mu\text{-}C_{10}H_{10}N_2)$ and $(LFePy)_2(\mu\text{-}C_{10}H_{10}N_2)$ that each predicted δ = 0.57-0.61 mm/s rather than the experimentally observed δ = 0.76-0.77 mm/s. Note that the larger deviation in the calculated quadrupole splitting is typical, because this is a more sensitive parameter and the agreement is not usually as good.[8]

The calculations predict that the higher isomer shift corresponds to the tetrahedral iron site, and the lower isomer shift corresponds to the π-allyl bound iron site. These assignments agree with the ones proposed on the basis of literature comparisons and bond distances. Comparison of different spin states shows that the septet state (S_{total} = 3) is lowest in energy; other spin states were either >40 kJ/mol higher in energy or did not converge. Since $(L'FePy)_2(\mu\text{-}C_{10}H_{10}N_2)$ has high-spin iron atoms with a very similar geometry as Fe1, it is reasonable to anticipate that Fe1 is also high-spin iron(II) (S_{Fe1} = 2). This would make Fe2 intermediate-spin (S_{Fe2} = 1), which agrees with the lower magnetic moment in compound **2**.

Table S3. Computational results

Compound	multiplicity	E (Hartrees)	E (kJ/mol)	rel E (kJ/mol)	calcd IS (mm/s)	calcd QS (mm/s)
					0.603	0.916
1A	9	-5480.60552	-14396218		0.577	0.884
					0.592	0.885
1B	9	-5480.62081	-14396258		0.592	0.926
					0.593	1.764
2	9	-4983.44145	-13090289	110	0.493	1.564
					0.623	-1.139
2	7	-4983.48317	-13090399	0	0.525	-0.888
					0.619	1.183
2	5	-4983.45634	-13090328	70	0.495	-1.525
2	3	didn't converge				
2	1	didn't converge				

References

[1] Neese, F. *ORCA*, version 3.0, MPI for Chemical Energy Conversion, Mülheim a.d. Ruhr, Germany, 2013. http://cec.mpg.de/forum/

[2] Tao, J. M. Perdew, J. P. Staroverov, V. N.; Scuseria, G. E. *Phys. Rev. Lett.* **2003**, *91*, 146401.

[3] Weigend, F; Ahlrichs, R. *Phys. Chem. Chem. Phys.* 2005, *7*, 3297.

[4] Römelt, M.; Ye, S.; Neese, F. *Inorg. Chem.* **2009**, *48*, 784.

[5] (a) Grimme, S., *J. Comput. Chem.* **2004**, *25*, 1463. (b) Grimme, S., *J. Comput. Chem.* **2006**, *27*, 1787. (c) Grimme, S.; Antony, J.; Ehrlich, S.; Krieg, H., *J. Chem. Phys.* **2010**, *132*, 154104.

[6] Massa, *Crystal Structure Determination*, Springer, New York, 2000

[7] Bittner, M. M.; Kraus, D.; Lindeman, S. V.; Popescu, C. V.; Fiedler, A. T. *Chem. Eur. J.* **2013,** *19*, 9686-9698.

[8] Neese, F. *J. Biol. Inorg. Chem.* **2006**, *11*, 702; Neese, F. *Coord. Chem. Rev.* **2009**, *253*, 526.